expansions," *IEEE Trans. Microwave Theory Tech.*, vol. 42, pp. 2412–2422, Dec. 1994.
[3] G. Wang and G. W. Pan, "Full wave analysis of microstrip floating line structures by wavelets expansion method," *IEEE Trans. Microwave Theory Tech.*, vol. 43, pp. 131–142, Jan. 1995.
[4] J. C. Goswami, A. K. Chan, and C. K. Chui, "On solving first-kind integral equations using wavelets on a bounded interval," *IEEE Trans. Antennas Propagat.*, vol. 43, pp. 614–622, June 1995.
[5] G. Oberschmidt, M. Behrens, and A. F. Jacob, "Comparison of spline-based wavelets for the analysis of microstrip lines," in *PIERS*, Innsbruck, Austria, July 1996, p. 581.
[6] K. F. Sabet, "Wavelet-based modeling of microwave circuits and antennas," presented at the Proc. Applicat. Wavelets Electromagnetics Workshop, San Francisco, CA, June 1996, ch. 3.
[7] S. G. Mallat, "A theory for multiresolution signal decomposition: The wavelet representation," *IEEE Trans. Pattern Anal. Machine Intell.*, vol. 11, pp. 674–693, July 1989.
[8] I. Daubechies, *Ten Lectures on Wavelets.* Philadelphia: SIAM, 1992.
[9] C. K. Chui and J. Z. Wang, "On compactly supported spline wavelets and a duality principle," *Trans. Amer. Math. Soc.*, vol. 330, no. 2, pp. 903–915, 1992.
[10] U. V. Gothelf and A. Østergaard, "Full-wave analysis of a two slot microstrip filter using a new algorithm for computation of the spectral integrals," *IEEE Trans. Microwave Theory Tech.*, vol. 41, pp. 101–108, Jan. 1993.
[11] R. H. Jansen and W. Wertgen, "A 3D field-theoretical simulation tool for the CAD of mm-wave MMIC's," *Alta Freq.*, vol. 47, no. 5, pp. 203–216, June 1988.
[12] T. K. Sarkar, Z. A. Marićević, and M. Kahrizi, "An accurate de-embedding procedure for characterizing discontinuities," *Int. J. Microwave Millimeter-Wave Computer-Aided Eng.*, vol. 2, no. 3, pp. 135–143, 1992.

The Generalized TLM-Based FDTD Modeling of Frequency-Dependent and Anisotropic Media

Zhizhang Chen and Jian Xu

***Abstract*— A generalization of the previously proposed transmission-line matrix (TLM)-based finite-difference time-domain (FDTD) method is presented for modeling frequency-dependent and anisotropic media. The generalized scheme incorporates electric- and magnetic-flux densities in addition to variable mesh sizes. Since it is in an FD form, modeling techniques developed for the conventional FDTD can be easily adapted into the proposed TLM-based technique. In this paper, a modified z-transform technique for frequency-dependent media is implemented, and a two-dimensional (2-D) full-wave technique for guided-wave structures is developed. In all the FDTD computations, no conversions between the field quantities and TLM circuit parameters such as open- and short-circuited stubs are required.**

***Index Terms*—Anisotropic, FDTD, frequency dependent, TLM.**

I. Introduction

Time-domain numerical methods have been shown to be powerful for solving electromagnetic related problems. These time-domain methods have received growing attention because of their versatility and simplicity. Two widely employed techniques so far are the finite-difference time-domain (FDTD) method of the Yee's grid [1] and the transmission-line matrix (TLM) method initially proposed by Johns [2]. The FDTD method is fairly easy to understand and implement, as it is the direct approximation of the Maxwell's equations. While the TLM, which uses the analogy between voltage and current waves in a transmission-line network and electromagnetic waves in space, is with less numerical dispersion. However, the TLM requires a conversion between the field quantities and circuit parameters to obtain the appropriate scattering matrix. For most of the cases, the conversions are not complicated, but sometimes they are not very straightforward and not easily understood, e.g., derivations of various impedances and open/short stub parameters related to variable grid sizes and medium inhomogeneity. To circumvent the problem, an FDTD and TLM combined technique—the TLM-based FDTD method equivalent to the TLM symmetrical condensed node—was proposed by Chen, Ney, and Hoefer [3], [4] while the work for the TLM expanded node was reported earlier by Voelker and Lomax [5].

The TLM-based FDTD is essentially the formulation of the TLM method in an FDTD fashion. It reveals the exact correspondence between the TLM and FDTD methods and the alternative ways of realizing the TLM concepts. Subsequent work on the more general correspondence was shown in [6]. The accuracy and dispersion comparisons between the TLM-based FDTD and the other FDTD schemes were presented in [7]. The TLM-based FDTD is found to have less numerical dispersion than the Yee's FDTD, but requires a little more memory space.

In this paper, the previously proposed TLM-based FDTD [3] is further exploited and generalized to include frequency dependence and anisotropics of a medium. Electromagnetic flux quantities are *directly* incorporated into the FDTD scheme and, therefore, a wide range of different media can be tackled. In this paper, frequency-dependent and anisotropic media are specifically treated. The successful applications of the technique shown in the following sections demonstrate the flexibility of the proposed FDTD method with its ease in adapting a different modeling scheme, e.g., the z-transform technique and the two-dimensional (2-D) full-wave technique. In all the proposed FDTD computations, no conversions between the field quantities and the TLM circuit parameters and stub-related operations are required. In addition, a normalizing procedure is also introduced to account for variable mesh sizes.

II. The Generalization of the TLM-Based FDTD Formulation

In a general three-dimensional (3-D) case, Maxwell's curl equations in a stationary and sourceless medium can be expressed in the rectangular coordinates. For instance, for D_x and B_y

$$\frac{\partial D_x}{\partial t} = \frac{\partial H_x}{\partial y} - \frac{\partial H_y}{\partial z} - \sigma_{ey} E_x \tag{1}$$

$$\frac{\partial B_y}{\partial t} = \frac{\partial E_z}{\partial x} - \frac{\partial E_x}{\partial z} - \sigma_{my} H_y \tag{2}$$

where σ_e and σ_m are, respectively, the equivalent electric and magnetic conductivities. Note that unlike the TLM-based FDTD developed so far, the flux densities are used in the equations.

Following the conventional notation, a function of the discretized space and time is denoted as

$$F(i\,\delta x,\, j\,\delta y,\, k\,\delta z,\, n\,\delta t) = F^n(i,\, j,\, k). \tag{3}$$

Manuscript received October 4, 1996; revised February 13, 1998. This work was supported in part by the Natural Sciences and Engineering Research Council of Canada.

Z. Chen is with the Department of Electrical and Computer Engineering, Daltech, Dalhousie University, Halifax, N.S., Canada B3J 2X4.
J. Xu is with Phase Atlantic Ltd., Moncton, N.B., Canada E1C 9N1.
Publisher Item Identifier S 0018-9480(98)03153-6.

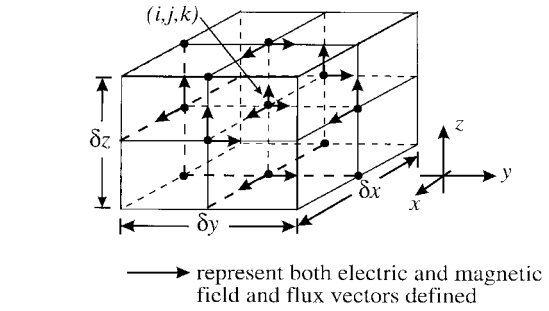

(a)

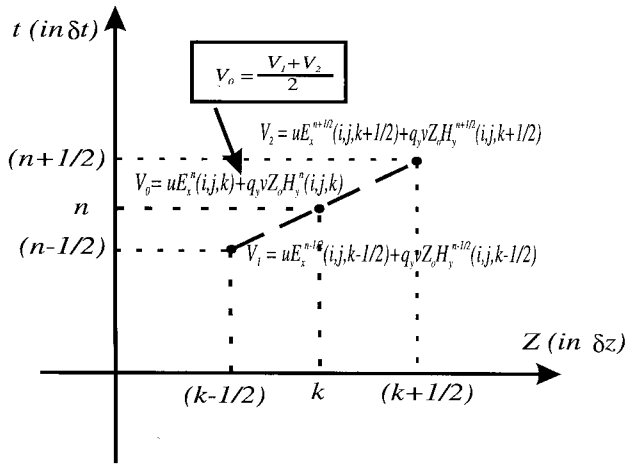

(b)

Fig. 1. (a) Grid arrangement for the TLM-based FDTD scheme. (b) Diagram illustrating the averaging process.

Here, δt is the time step, and δx, δy, and δz are the spatial steps. The spatial steps are not necessarily equal for a nonuniform grid.

The grid arrangement for a 3-D cell is the same as that presented in [3] with the exception that, now at the center of the 3-D cell, not only the six field components of $\boldsymbol{E}$, $\boldsymbol{H}$ are defined, but more importantly, their corresponding flux densities $\boldsymbol{D}$ and $\boldsymbol{B}$ are also defined [see Fig. 1(a)]. Again, at the boundary surfaces of each 3-D cell, only the field components tangential to the surfaces are considered.

Similarly to that developed in [3], the recursive FDTD computation process at each time step involves the following two half-time-step operations:

1) updating of flux components at the center of a 3-D cell on the first half time step;
2) updating of the field components at the boundary surfaces of the cell on the second half-time step.

In 1), however, only the flux quantities are computed. Therefore, additional computations are required to update the field components at the center of a 3-D cell. The following details the whole computation process which also include a normalizing procedure to account for the use of variable mesh sizes.

A. Updating of Flux Components at the Center of a 3-D Cell

To update the flux components at the center, Maxwell's equations are applied. By simply finite-differencing Maxwell's equations, in respect to the center of a 3-D cell [denoted as (i, j, k)], an FD formulation can be obtained easily. For example, for D_x and B_y components, one can obtain

$$\left[D_x^n(i,j,k)+\frac{\sigma_{ex}\,\delta t}{2}E_x^n(i,j,k)\right] = D_x^{n-1}(i,j,k)-\frac{\sigma_{ex}\,\delta t}{2}E_x^{n-1}(i,j,k) - \frac{\delta t}{\delta z}\left[H_y^{n-1/2}\left(i,j,k+\frac{1}{2}\right)-H_y^{n-1/2}\left(i,j,k-\frac{1}{2}\right)\right] + \frac{\delta t}{\delta y}\left[H_z^{n-1/2}\left(i,j+\frac{1}{2},k\right)-H_z^{n-1/2}\left(i,j-\frac{1}{2},k\right)\right] \tag{4}$$

$$\left[B_y^n(i,j,k)+\frac{\sigma_{my}\,\delta t}{2}H_y^n(i,j,k)\right] = B_y^{n-1}(i,j,k)-\frac{\sigma_{my}\,\delta t}{2}H_y^{n-1}(i,j,k) + \frac{\delta t}{\delta x}\left[E_z^{n-1/2}\left(i+\frac{1}{2},j,k\right)-E_z^{n-1/2}\left(1-\frac{1}{2},j,k\right)\right] - \frac{\partial t}{\partial z}\left[E_x^{n-1/2}\left(i,j,k+\frac{1}{2}\right)-E_x^{n-1/2}\left(i,j,k-\frac{1}{2}\right)\right]. \tag{5}$$

The equations for the other components can be obtained in a similar way.

B. The Additional Computations: Updating of Field Components at the Center of a 3-D Cell from the Flux Quantities

Once the flux quantities are obtained, the E and H at the center of a cell can be updated through a solution of the medium constitutive relationship (which is supposed to be known or can be found) as follows:

$$\mathbf{D}=\mathbf{D}(\mathbf{E},\mathbf{H}) \tag{6}$$

$$\mathbf{B}=\mathbf{B}(\mathbf{E},\mathbf{H}). \tag{7}$$

The different types of media present different forms of constitutive relationships. They will be described in more details in Section IV on the individual problem basis.

C. Updating of Field Components at the Boundary Surfaces of a 3-D Cell

After the field components at the center of a 3-D cell are determined, the field components at the boundary surfaces of the cell can be updated through a special averaging process in both space and time.

Suppose that a normalizing length δl is selected, which is less than or equal to the smallest cell size over the grid. A time step $\delta t = s\,\delta l/c_o$ can then be chosen, with c_o being the speed of light in vacuum. s is the so-called stability factor which determines the numerical dispersion characteristics and stability as shown in [7]. When the dimensional factor $s = 0.5$, the FDTD becomes exactly equivalent to the 3-D TLM symmetrical condensed node.

The mesh size of a 3-D cell of $\delta x \times \delta y \times \delta z$ can then be normalized to Δl as follows:

$$u=\delta x/\delta l \qquad (\geq 1) \tag{8}$$

$$v=\delta y/\delta l \qquad (\geq 1) \tag{9}$$

$$w=\delta z/\delta l \qquad (\geq 1). \tag{10}$$

A set of equations can now be obtained based on the TLM scheme, or equivalently, the averaging process described in [6]. Another way of obtaining them is by so-called "characteristic decomposition" [8]. For example, at surface point $(i, j, k+\frac{1}{2})$, which interfaces the cell centered at (i, j, k) and the cell centered at $(i, j, k+1)$, one

can have (11) and (12), shown at the bottom of the page. Here, $Z_o = \sqrt{\mu_o/\varepsilon_o}$ is the free-space impedance and q_y is a cell-size related constant which determines the type of TLM node the proposed FDTD is equivalent to. For instance, selecting $q_y = 1$ will make the proposed FDTD equivalent to the TLM symmetrical condensed node while using $q_y = \mu_y uw/v$ will make the FDTD equivalent to the TLM hybrid symmetrical condensed node. These equivalencies can be easily seen in [6].

The averaged quantities are $uE_x \pm q_y v Z_o H_y$. They are averaged over the z-direction. Equation (11) is the result of averaging over the cell centered at (i, j, k) while (12) is the result of averaging over the neighboring cell centered at $(i, j, k+1)$. Fig. 1(b) shows the averaging diagram. As to the $\pm$ signs, $uE_x + q_y v Z_o H_y$ is used in (11) since $\boldsymbol{E_x} \times \boldsymbol{H_y}$ points to $(i, j, k+\frac{1}{2})$ at which the surface field values are to be found. In (12), $uE_x - q_y v Z_o H_y$ is taken since $\boldsymbol{E_x} \times (-\boldsymbol{H_y})$ points to $(i, j, k+\frac{1}{2})$.

The solutions of (11) and (12) read as (13) and (14), shown at the bottom of the next page.

The above equations permit the update of E_x and H_y at the boundary surface $z = (k+\frac{1}{2})\delta z$ in terms of field values of the previous time step, at the boundary surfaces between two cells, and at the centers of two neighboring cells.

The equations for the other components can be obtained in a similar way.

To facilitate the efficient programming and fast computation, (4) and (5), which are used for updating the field components at the center of a 3-D cell, can be rewritten in the following form:

$$\left[\frac{vw}{u}\,\frac{uD_x^n(i,j,k)}{\varepsilon_o} + g_x uE_x^n(i,j,k)\right] = \frac{vw}{u}\,\frac{uD_x^{n-1}(i,j,k)}{\varepsilon_o} - g_x uE_x^{n-1}(i,j,k) - s[vZ_oH_y^{n-1/2}(i,j,k+\tfrac{1}{2}) - vZ_oH_y^{n-1/2}(i,j,k-\tfrac{1}{2})] + s[wZ_oH_z^{n-1/2}(i,j+\tfrac{1}{2},k) - wZ_oH_z^{n-1/2}(i,j-\tfrac{1}{2},k)] \tag{15}$$

$$\left[\frac{uw}{v}\,\frac{vZ_oB_y^n(i,j,k)}{\mu_o} + r_y vZ_oH_y^n(i,j,k)\right] = \left[\frac{uw}{v}\,\frac{vB_y^{n-1}(i,j,k)}{\mu_o} - r_y vZ_oH_y^{n-1}(i,j,k)\right] + s[wE_z^{n-1/2}(i+\tfrac{1}{2},j,k) - wE_z^{n-1/2}(i-\tfrac{1}{2},j,k)] - s[uE_x^{n-1/2}(i,j,k+\tfrac{1}{2}) - uE_x^{n-1/2}(i,j,k-\tfrac{1}{2})] \tag{16}$$

where $g_x = (vw/u)(\sigma_{ex}\,\delta t/\varepsilon_o)$ and $r_y = (uw/v)(\sigma_{mx}\,\delta t/\mu_o)$.

The reason for this reformulation is that together with (11) and (12), uE_x, wE_z, vZ_oH_y, and wZ_oH_z can now be considered as the quantities for computation instead of E_x, E_z, H_y, and H_z. The computation counts are thus reduced.

Careful examinations of all the FDTD equations indicate that many terms are identical and need to be computed only once. In the averaging equations such as (11) and (12), $uE_x \pm q_y vZ_oH_y$ is one of them. As a result, the computation counts are further reduced and can be found to be the same as the recently developed symmetrical super-condensed node (SSCN) [9] since in both cases no stub-related operations are required. Yet in the proposed TLM-based FDTD scheme, no conversions between the constitutive parameters and circuit parameters used in the TLM model are required. Moreover, because of the proposed FDTD form, any other techniques developed for the Yee's FDTD can easily be adapted as shown in Section III.

III. Numerical Results

Two examples are computed here: firstly, propagation in frequency-dependent media; secondly, the dispersion of a microstrip line with an electrically and magnetically anisotropic substrate. In all the computations, $Z_o = \sqrt{\mu_o/\varepsilon_o}$ and $q's = 1$ are used for simplicity as they are constant independent of the medium types and mesh sizes.

Example 1.—A Plane Wave Incident on the Half-Space Filled With Second- and Fourth-Order Lorentz Medium: A plane wave propagating in the z-direction was considered. The half-space $z < 0$ is air while the other half $z > 0$ is filled with the second-order dispersive Lorentz medium whose dispersion is specified by

$$\epsilon(\omega) = \epsilon_\infty - \frac{(\epsilon_s - \epsilon_\infty)}{1 + j2\delta\left(\frac{\omega}{\omega_o}\right) - \left(\frac{\omega}{\omega_o}\right)^2} \tag{17}$$

where $\epsilon_s = \epsilon(f=0)$, $\epsilon_\infty = \epsilon(f=\infty)$, ω_o is the resonant frequency and δ is the damping coefficient. Their values are taken from [11]

$$\epsilon_s = 2.25\epsilon_o$$
$$\epsilon_\infty = \epsilon_o$$
$$\omega_o = 4.0 \times 10^{16}\ \text{rad/s}$$
$$\delta = 0.14 \times 10^{16}\ \text{s}^{-1}.$$

In order to apply (17) to the time-domain simulation, a frequency-to-time conversion is required. In this case, the modified Z-transform described in [10] is employed. The result is the recursive time-domain constitutive relationship between $\boldsymbol{E}$ and $\boldsymbol{D}$ which replaces the constitutive relationships (6) and (7) in the following proposed FDTD computation:

$$E^n = \frac{\frac{1}{\epsilon_s} D^n - S_L^{n-1}}{\epsilon_\infty} \tag{18}$$

$$S^{n-1} = \text{c1} \cdot S_L^{n-2} - \text{c2} \cdot S_L^{n-3} + \text{c3} \cdot E^{n-1} \tag{19}$$

$$H^n = \frac{B^n}{\mu_o} \tag{20}$$

where c1, c2, and c3 are constants, as defined in [10].

The above equations permit the updating of the E- and H-field components from the flux density D and B at the center of a 3-D cell.

To demonstrate the accuracy of the proposed method, the wide-band reflection coefficient was computed with the FDTD method. A single impulse having a spectrum from dc to infinity was injected so as to be normally incident on the interface. Data was taken at every time step ($\delta t = 2.0 \times 10^{-19}$ s) from a fixed observation point on the vacuum side of the interface. Fig. 2 compares the FDTD-computed magnitude and phase of the reflection coefficients as a function of frequency to the exact solution [11]. The deviation from

$$\frac{[uE_x^{n+1/2}(i,j,k+\frac{1}{2}) + q_y vZ_oH_y^{n+1/2}(i,j,k+\frac{1}{2})] + [uE_x^{n-1/2}(i,j,k-1/2) + q_y vZ_oH_y^{n-1/2}(i,j,k-\frac{1}{2})]}{2} = uE_x^n(i,j,k) + q_y vZ_oH_y^n(i,j,k) \tag{11}$$

$$\frac{[uE_x^{n+1/2}(i,j,k+\frac{1}{2}) - q_y vZ_oH_y^{n+1/2}(i,j,k+\frac{1}{2})] + [uE_x^{n-1/2}(i,j,k+\frac{3}{2}) - q_y vZ_oH_y^{n-1/2}(i,j,k+\frac{3}{2})]}{2} = uE_x^n(i,j,k+1) - q_y vZ_oH_y^n(i,j,k+1) \tag{12}$$

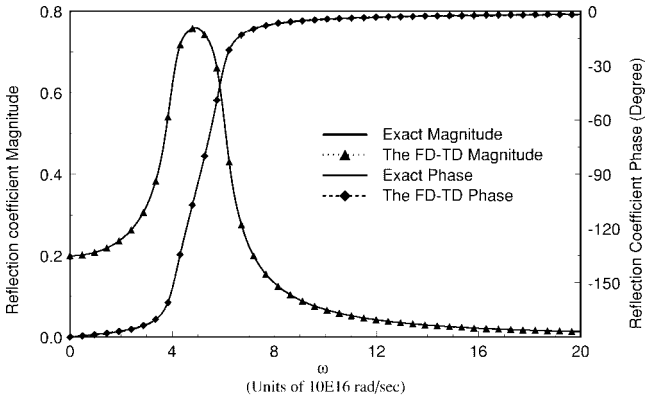

Fig. 2. Comparison of the FDTD and exact results from dc to 30 000 THz for the reflection coefficient of a half-plane made of Lorentz medium.

the exact solution over the complete range of dc to 3×10^{16} Hz is not visible.

To further demonstrate the effectiveness of the proposed FDTD scheme, an attempt was also made to compute the wave incident on a higher order dispersive medium, namely, a fourth-order dispersive medium. The geometry and parameters was selected the same as those used in [12]. The excitation is a Gaussian-pulse plane wave. The pulse initially has a spatial width of 256 cells between the 0.001 amplitude points and contains energy of frequency up to 80 GHz.

Spatial plots of electric field versus positions for the pulse are shown in Fig. 3 as the pulse is reflected from the interface and propagates in the dispersive medium. The extremely dispersive nature of the medium is clearly visible. Good agreement is found between these results and those presented in [12].

Example 2. Calculation of Dispersion Relation of a Microstrip Line With an Anisotropic Substrate: In this example, a microstrip line deposited on an electrically and magnetically anisotropic substrate is considered (see Fig. 4). The geometry and parameters are taken to be the same as those used in [13]. The constitutive relations for the substrate are then

$$\mathbf{D} = [\epsilon]\mathbf{E} \tag{21}$$

$$\mathbf{B} = [\mu]\mathbf{H} \tag{22}$$

where

$$\begin{aligned}
\varepsilon_{11} &= \varepsilon_{x1} \cos^2\theta + \varepsilon_{z1} \sin^2\theta \\
\varepsilon_{33} &= \varepsilon_{x1} \sin^2\theta + \varepsilon_{z1} \cos^2\theta \\
\varepsilon_{22} &= \varepsilon_{y1} \\
\varepsilon_{13} &= j\varepsilon_{31} = (\varepsilon_{z1} - \varepsilon_{x1}) \sin\theta \cos\theta \\
\mu_{11} &= \mu_{x2} \cos^2(\theta + \Delta\theta) + \mu_{z2} \sin^2(\theta + \Delta\theta) \\
\mu_{33} &= \mu_{x2} \sin^2(\theta + \Delta\theta) + \mu_{z2} \cos^2(\theta + \Delta\theta) \\
\mu_{22} &= \mu_{y2}
\end{aligned}$$

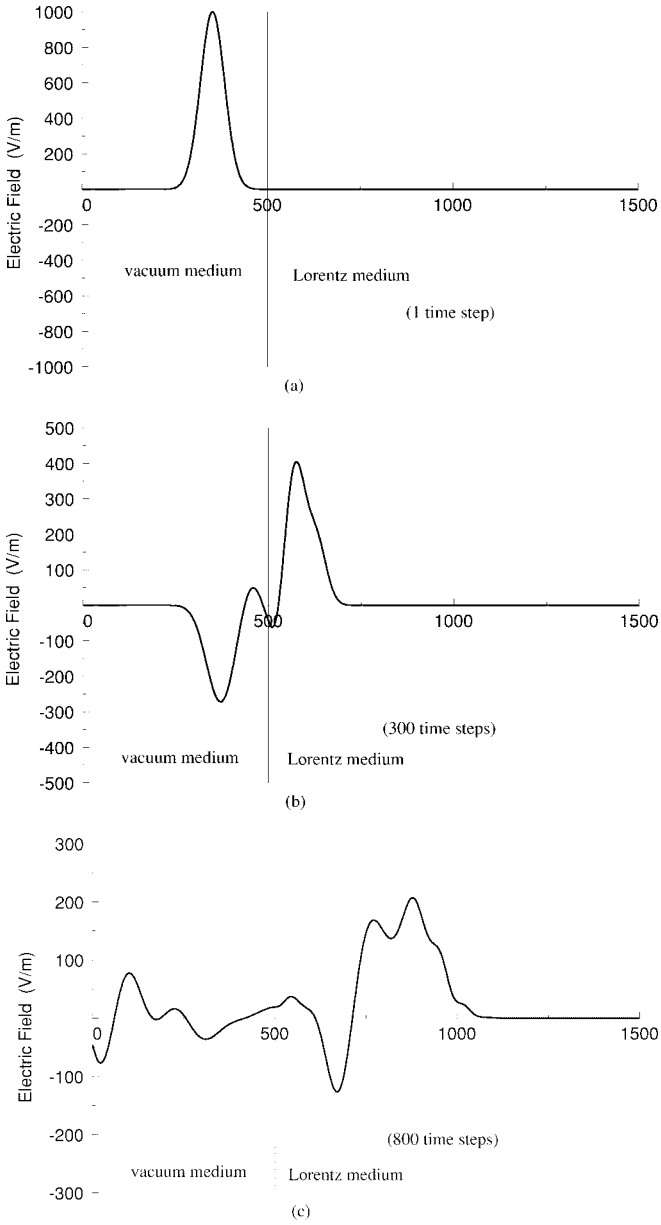

Fig. 3. Electric field versus position for a pulse plane wave incident from vacuum onto the fourth-order dispersive medium.

and

$$\mu_{13} = j\mu_{31} = (\mu_{z2} - \mu_{x2}) \sin(\theta + \Delta\theta) \cos(\theta + \Delta\theta).$$

θ and $\theta + \Delta\theta$ represent the rotation angles for the permittivity and permeability tensors in the x–z plane.

To compute the dispersion in an efficient way, the 2-D full-wave technique recently developed on the Yee's FDTD grid [14] was

$$\begin{aligned}
uE_x^{n+1/2}(i, j, k+\tfrac{1}{2}) &= -0.5[uE_x^{n-1/2}(i, j, k-\tfrac{1}{2}) + q_y v Z_o H_y^{n-1/2}(i, j, k-\tfrac{1}{2})] - 0.5[uE_x^{n-1/2}(i, j, k+\tfrac{3}{2}) - q_y v Z_o H_y^{n-1/2}(i, j, k+\tfrac{3}{2})] \\
&\quad - +[uE_x^{n}(i, j, k) + q_y v Z_o H_y^{n}(i, j, k)] + [uE_x^{n}(i, j, k+1) - q_y v Z_o H_y^{n}(i, j, k+1)] \qquad (13) \\
q_y v Z_o H_y^{n+1/2}(i, j, k+\tfrac{1}{2}) &= -0.5[uE_x^{n-1/2}(i, j, k-\tfrac{1}{2}) + q_y v Z_o H_y^{n-1/2}(i, j, k-\tfrac{1}{2})] \\
&\quad + 0.5[uE_x^{n-1/2}(i, j, k+\tfrac{3}{2}) - q_y v Z_o H_y^{n-1/2}(i, j, k+\tfrac{3}{2})] \\
&\quad + [uE_x^{n}(i, j, k) + q_y v Z_o H_y^{n}(i, j, k)] - [uE_x^{n}(i, j, k+1) - q_y v Z_o H_y^{n}(i, j, k+1)] \qquad (14)
\end{aligned}$$

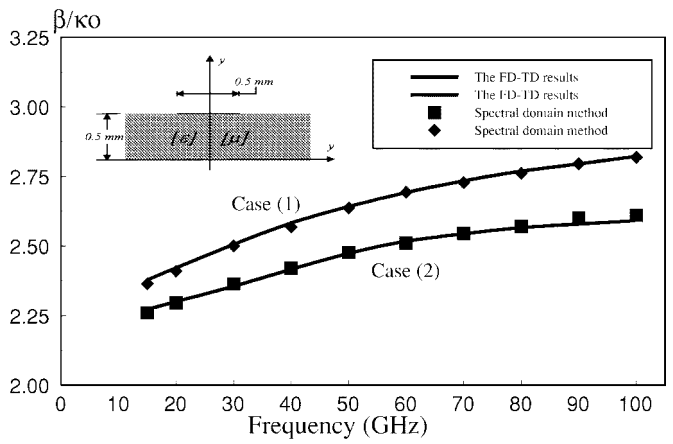

Fig. 4. Calculated dispersion of the open microstrip line with simultaneously rotated material axes.

adapted into the proposed FDTD technique. In the same way as that described in [14], one can assume

$$[D_x,\ D_y,\ B_z] = [D_x(x,\ y),\ D_y(x,\ y),\ B_z(x,\ y)]je^{-j\beta z} \quad (23)$$

$$[B_x,\ B_y,\ D_z] = [B_x(x,\ y),\ B_y(x,\ y),\ B_z(x,\ y)]e^{-j\beta z} \quad (24)$$

$$[E_x,\ E_y,\ H_z] = [E_x(x,\ y),\ E_y(x,\ y),\ H_z(x,\ y)]je^{-j\beta z} \quad (25)$$

$$[H_x,\ H_y,\ E_z] = [H_x(x,\ y),\ H_y(x,\ y),\ E_z(x,\ y)]e^{-j\beta z}. \quad (26)$$

Substitution of these equations into the proposed FDTD formulation and application of $\Delta z \to 0$ leads to a 2-D full-wave TLM-based FDTD formulation for guided wave structures. For instance, (15) becomes

$$\begin{aligned}\left[\frac{vw}{u}\,\frac{uD_x^n(i,\ j)}{\varepsilon_o} + g_x u E_x^n(i,\ j)\right] &= vw\,\frac{DE_x^n(i,\ j)}{\varepsilon_o} \\ &= \frac{vw}{u}\,\frac{uD_x^{n-1}(i,\ j)}{\varepsilon_o} - g_x u E_x^{n-1}(i,\ j) - \beta v Z_o H_y^{n-1/2}(i,\ j) \\ &\quad + [wZ_o H_z^{n-1/2}(i,\ j+\tfrac{1}{2}) - wZ_o H_z^{n-1/2}(i,\ j-\tfrac{1}{2})] \quad (27)\end{aligned}$$

and (13) becomes

$$vZ_o H_y^{n+1/2}(i,\ j) = 2vZ_o H_y^{n-1/2}(i,\ j) - vZ_o H_y^{n-1/2}(i,\ j). \quad (28)$$

Note that the third-dimension z is now closed and index k disappears. For the other components, the equations can be obtained in a similar way.

Fig. 4 shows the calculated dispersion characteristics of the open microstrip line. Two cases are computed: 1) $\theta = 0$, $\Delta\theta = 0$ and 2) $\theta = 15^\circ$, $\Delta\theta = 58^\circ$. The results are shown against the results obtained with the spectrum domain technique [13]. They are found to be in very good agreement. Due to the symmetry, only half of the structure was computed with a magnetic wall placed at $x = 0$. An 8 $\times$ 8 nonuniform grid is used. Coordinates of the grid mesh in x- and y-directions are 0, 0.125, 0.25, 0.375, 0.5, 0.63, 0.93, 1.93, 5.0 mm and 0, 0.125, 0.25, 0.375, 0.5, 0.63, 1.0, 2.0, 5.0 mm. 10 000 time iterations are used. On a DEC ALPHA 600/266 MHz workstation, calculations for each frequency point take about 40 s.

IV. Discussions and Conclusions

In this paper, the TLM-based FDTD formulation for Maxwell's equations is generalized for modeling frequency-dependent and anisotropic media. Both electric and magnetic flux quantities and variable mesh sizes are incorporated into the algorithm. The method is still a TLM-based technique realizing the TLM concepts, but is formulated in an FDTD fashion. As a result, various techniques which have been developed for the other FDTD methods (such as the Yee's FDTD) can be easily adapted into the TLM-based method. In this paper, the implementation of the modified Z-transform technique for the frequency-dependent media and the compact 2-D full-wave technique for guided-wave structures are demonstrated. In all these computations, no conversions between the field quantities and the TLM circuit parameters and stub-related operations are required. Finally, it is worth mentioning that the authors have also successfully adapted a nonlinear modeling scheme and perfectly matched layer (PML) into the TLM-based FDTD [15].

Acknowledgment

The authors are thankful to Dr. J. M. Chuang for his help in setting up the computing facilities.

References

[1] K. S. Yee, "Numerical solution of initial boundary value problems involving Maxwell's equations," *IEEE Trans. Antennas Propagat.*, vol. AP-14, pp. 302–307, May 1966.

[2] P. B. Johns, "A symmetrical condensed node for the TLM method," *IEEE Trans. Microwave Theory Tech.*, vol. MTT-35, pp. 370–377, Apr. 1987.

[3] Z. Chen, M. M. Ney, and W. J. R. Hoefer, "A new finite-difference time-domain formulation and its equivalence with the TLM symmetrical condensed node," *IEEE Trans. Microwave Theory Tech.*, vol. 39, pp. 2160–2169, Dec. 1991.

[4] Z. Chen, "The generalized TLM based finite-difference time-domain method and its applications to frequency-dependent and anisotropic media," in *IEEE Int. Microwave Symp. Dig.*, San Francisco, CA, June 17–21, 1996, pp. 435–438.

[5] R. Voelker and R. J. Lomax, "A finite-difference transmission line matrix method incorporating a nonlinear device model," *IEEE Trans. Microwave Theory Tech.*, vol. 38, pp. 302–312, Mar. 1990.

[6] J. Hang and R. Vahldieck, "Direct derivation of TLM symmetrical condensed node and hybrid symmetrical condensed node from Maxwell's equations using centered differencing and averaging," *IEEE Trans. Microwave Theory Tech.*, vol. 42, pp. 2554–2561, Dec. 1994.

[7] K. L. Shlager, J. G. Maloney, S. L. Ray, and A. P. Peterson, "Relative accuracy of several finite-difference time-domain methods in two and three dimensions," *IEEE Trans. Antennas Propagat.*, vol. 41, pp. 1732–1736, Dec. 1993.

[8] J. LoVetri and N. R. S. Simons, "A class of symmetrical condensed node TLM methods derived directly from Maxwell's equations," *IEEE Trans. Microwave Theory Tech.*, vol. 41, pp. 1419–1428, Aug. 1993.

[9] V. Trenkic, C. Christopoulos, and T. M. Benson, "Theory of the symmetrical super-condensed node for the TLM method,"*IEEE Trans. Microwave Theory Tech.*, vol. 43, pp. 1342–1348, June 1995.

[10] D. Sullivan, "Frequency-dependent FDTD method using Z transform," *IEEE Trans. Antennas Propagat.*, vol. 40, pp. 1223–1230, Oct. 1992.

[11] P. Goorjian and A. Taflove, "Direct time integration of Maxwell's equations in linear dispersive media with absorption for scattering and propagation of femtosecond electromagnetic pulses," *Opt. Lett.*, vol. 16, no. 18, pp. 1412–1414, Sept. 1991.

[12] R. Luebbers and F. P. Hunsberger, "FDTD for Nth-order dispersive media," *IEEE Trans. Antennas Propagat.*, vol. 40, pp. 1297–1301, Nov. 1992.

[13] Y. Chen and B. Beker, "Dispersion characteristics of open and shielded microstrip lines under a combined principal axes rotation of electrically and magnetically anisotropic substrates," *IEEE Trans. Microwave Theory Tech.*, vol. 41, pp. 673–679, Apr. 1993.

[14] S. Xiao and R. Vahldieck, "An efficient 2-D FDTD algorithm using real variables," *IEEE Microwave Guided Wave Lett.*, vol. 3, pp. 127–129, May 1993.

[15] Z. Chen and J. Xu, "The TLM based FDTD summary of recent progress," *IEEE Microwave Guided Wave Lett.*, vol. 7, pp. 12–14, Jan. 1997.